Brain Imaging and Behavior
https://doi.org/10.1007/s11682-020-00420-5

ORIGINAL RESEARCH

Structural and functional brain changes in hepatic and neurological Wilson disease

Sule Tinaz[1,2] · Jagriti Arora[3] · Keerthana Nalamada[1] · Ana Vives-Rodriguez[1] · Mine Sezgin[1,4] · Daphne Robakis[1,5] · Amar Patel[1] · R. Todd Constable[3] · Michael L. Schilsky[6]

Accepted: 9 November 2020

Abstract

Wilson disease (WD) can manifest with hepatic or neuropsychiatric symptoms. Our understanding of the in vivo brain changes in WD, particularly in the hepatic phenotype, is limited. Thirty subjects with WD and 30 age- and gender-matched controls participated. WD group underwent neuropsychiatric assessment. Unified WD Rating Scale neurological exam scores were used to determine neurological (WDN, score > 0) and hepatic-only (WDH, score 0) subgroups. All subjects underwent 3 Tesla anatomical and resting-state functional MRI. Diffusion tensor imaging (DTI) and susceptibility-weighted imaging (SWI) were performed only in the WD group. Volumetric, DTI, and functional connectivity analyses were performed to determine between-group differences. WDN and WDH groups were matched in demographic and psychiatric profiles. The entire WD group compared to controls showed significant thinning in the bilateral superior frontal cortex. The WDN group compared to control and WDH groups showed prominent structural brain changes including significant striatal and thalamic atrophy, more subcortical hypointense lesions on SWI, and diminished white matter integrity in the bilateral anterior corona radiata and corpus callosum. However, the WDH group also showed significant white matter volume loss compared to controls. The functional connectivity between the frontostriatal nodes was significantly reduced in the WDN group, whereas that of the hippocampus was significantly increased in the WDH group compared to controls. In summary, structural and functional brain changes were present even in neurologically non-manifesting WD patients in this cross-sectional study. Longitudinal brain MRI scans may be useful as biomarkers for prognostication and optimization of treatment strategies in WD.

Keywords Wilson disease · Volumetric MRI · DWI · Resting-state fMRI · Functional connectivity

Introduction

Wilson disease (WD) is a rare metabolic disorder of autosomal recessive inheritance characterized by *ATP7B* gene mutations that leads to copper accumulation particularly in the liver and later in the brain (Bennett and Hahn 2011). Toxic accumulation of copper causes oxidative stress and eventually cell death (Członkowska et al. 2018).

Prevalence rates of WD vary between 1 in 30,000–100,000 and could be even higher (Gao et al. 2019; Schilsky 2017). WD can manifest with hepatic or neuropsychiatric symptoms, acutely or chronically. Diagnosing WD can be challenging due to the diverse nature of its presentation and genetics. The consequence of a missed or delayed diagnosis and treatment initiation may lead to irreversible morbidity and mortality (Walshe and Yealland 1993).

WD affects the basal ganglia (Fritzsch et al. 2014; Kozić et al. 2003; Litwin et al. 2013; Magalhaes et al. 1994;

✉ Sule Tinaz
sule.tinaz@yale.edu

1 Department of Neurology, Yale University School of Medicine, 15 York St, LCI Suite 710, New Haven, CT 06510, USA

2 Clinical Neurosciences Imaging Center, Yale University School of Medicine, New Haven, CT, USA

3 Department of Radiology and Biomedical Imaging, Yale University School of Medicine, New Haven, CT, USA

4 Istanbul Faculty of Medicine, Department of Neurology, Istanbul University, Istanbul, Turkey

5 Department of Neurology, State University of New York Downstate College of Medicine, Brooklyn, NY, USA

6 Departments of Medicine and Surgery, Sections of Digestive Diseases and Transplant and Immunology, Yale University School of Medicine, New Haven, CT, USA

Published online: 26 November 2020

Südmeyer et al. 2006; Yang et al. 2015; Zhong et al. 2019; Zhou et al. 2016; Zou et al. 2019) and other brain regions (Fritzsch et al. 2014; Litwin et al. 2013; Yang et al. 2015; Zhong et al. 2019; Zhou et al. 2016). These changes may be present in neurologically non-manifesting (Favrole et al. 2006; Kozić et al. 2003; Litwin et al. 2013) and presymptomatic cases (Litwin et al. 2013), as well as in heterozygous carriers (Tarnacka et al. 2009). WD also alters the functional organization of brain networks (Han et al. 2016; Jing et al. 2019). In most brain imaging studies to date, the hepatic and neurologic phenotypes of WD have been grouped together. Therefore, our understanding of the in vivo brain changes specifically in WD patients without neurological manifestations of the illness is limited. We aimed to fill this knowledge gap by characterizing the structural and functional brain changes of WD patients with and without neurological exam manifestations, and comparing these to matched controls. We hypothesized that not only the neurologically manifesting, but also the non-manifesting (i.e., hepatic-only) WD group will demonstrate atrophy and reduced functional connectivity (FC), especially in the basal ganglia, compared to controls. The WD phenotypes usually do not remain discrete and co-occurrence of hepatic and neurological symptoms would be expected on the disease continuum. Capturing the brain changes before the onset of neurological problems would thus be valuable in prognostication and treatment decisions.

Methods

Participants

The study was approved by the Human Research Protection Office of the Yale School of Medicine and conducted at the Yale University Magnetic Resonance Research Center (MRRC). All participants provided written informed consent and underwent screening for MRI safety. We included 30 participants with WD (19–71 years old) recruited from the WD clinic at the Yale New Haven Hospital and through advertisements posted by the Wilson Disease Association. Participants were diagnosed with WD according to the Leipzig criteria, having definitive scores >4 (Ferenci et al. 2003). Neuropsychiatric symptoms due to a process other than WD precluded participation. Liver cirrhosis was not an exclusion criterion, however, those with known portal hypertension were excluded to minimize the risk of encephalopathy. Participants were either on chelation or zinc treatment for their WD for at least one year.

We selected the age- and gender-matched control participants (19–58 years old) from a Yale MRRC database. Participants were recruited from the New Haven area. Participants were excluded if they had any neurologic or psychiatric illness, any medical condition affecting the central nervous system, or any major surgery.

Clinical assessment

We divided the WD patients into two groups: Hepatic-only (WDH) or neurologic (WDN) based on neurologic examination findings. We assessed the neurologic disease severity using the Unified WD Rating Scale (UWDRS) (Członkowska et al. 2007). The UWDRS part I rates consciousness, UWDRS II is the patient-assessed disability part, and UWDRS III is rater-determined by neurologic examination. We assigned all participants with a UWDRS III score > 0 to the WDN group and those with a score of 0 to the WDH group.

We used the Diagnostic Statistical Manual 5 Self-Rated Level 1 Cross-Cutting Symptom Measure (DSM-5 CCM) to assess the presence and severity of psychiatric symptoms (Clarke and Kuhl 2014). We used the Repeated Battery for Assessment of Neuropsychological Status (RBANS) for cognitive testing, which assesses immediate memory, visuospatial capabilities, language, attention, and delayed memory (Karantzoulis et al. 2013; Randolph et al. 1998). We evaluated executive function using the Trail Making Test (TMT) and Phonemic Fluency (letter F) (Strauss et al. 2006). The TMT has also been promoted as a bedside assessment of hepatic encephalopathy (Conn 1977; Torres et al. 2013).

MRI sequences

WD group

All participants underwent scanning in two different 3-Tesla Siemens Prisma scanners (Siemens Medical Systems, Erlangen, Germany) using a 64-channel head coil and identical sequences. After a localizer scan, we acquired a high-resolution whole-brain T1-weighted MPRAGE scan (TR = 2530 ms, TE =2.44 ms, TI = 900 ms, flip angle = 9°, FoV = 256 mm, voxel size = 1 mm^3). We collected four consecutive T2-weighted resting-state (rs) functional MRI (fMRI) scans with eyes closed each lasting 6 min (echo-planar pulse sequence, TR = 1000 ms, TE = 30 ms, flip angle = 52°, FoV = 216 mm, matrix size = 64 × 64, voxel size = 2.4 mm^3, 60 slices). Then, we collected T2-weighted susceptibility weighted imaging (SWI) scans to visualize the subcortical hypointense regions due to accumulation of paramagnetic substances (e.g., iron, copper) (TR = 27 ms, TE = 20 ms, flip angle = 15°, FoV = 220 mm, voxel size = 0.9 × 0.9 × 1.5 mm). In addition, we collected T2-weighted SPACE scans (TR = 3200 ms, TE = 408 ms, FoV 230 mm, voxel size = 0.4 × 0.4 × 0.9 mm, 192 slices) to evaluate for whole-brain gross structural abnormalities. Finally, we collected T2-weighted DTI scans to evaluate the integrity of the white matter tracts (fat saturated, TR = 4000 ms, TE = 77 ms, flip angle 1 = 90°, flip angle 2 = 180°, FoV = 216 mm, voxel size = 2.4 mm^3, maximum B value = 1000 s/mm^2, 64 diffusion gradients, 76 slices).

Control group

All participants underwent scanning in a 3-Tesla Siemens Tim Trio scanner (Siemens Medical Systems, Erlangen, Germany) using a 32-channel head coil. Each scanning session started with a localizer scan followed by a MPRAGE scan (TR = 2530 ms, TE =2.77 ms, TI = 1100 ms, flip angle = 7°, voxel size = 1 mm^3). We collected six consecutive T2-weighted rs-fMRI scans with eyes closed each lasting 5 min and 25 s (echo-planar pulse sequence, TR = 956 ms, TE = 30 ms, flip angle = 62°, FoV = 220 mm, matrix size = 64 × 64, voxel size = 2.5 mm^3, 51 slices).

Clinical data analysis

We assessed normal distribution of the clinical data using the Shapiro-Wilk test. We performed independent sample t-tests for normally distributed continuous variables and Mann Whitney U tests for non-normally distributed variables. We used chi-square tests for categorical variables. The statistical significance threshold was $p < 0.05$ for all tests. We used the SPSS 26 for Mac (IBM Corp., Armonk, NY, USA).

Subcortical volume and cortical thickness analysis

We used the standard processing pipeline in FreeSurfer (https://surfer.nmr.mgh.harvard.edu). Briefly, we used the subcortical volume-based stream (Fischl et al. 2002) and the cortical surface-based stream (Dale et al. 1999; Fischl et al. 1999; Fischl and Dale 2000) to obtain the individual subcortical volume and cortical thickness values, respectively. We inspected the outcomes of the skull-stripping, cortical tessellation, and subcortical segmentation stages for quality control.

Statistical analysis of subcortical volumes

We extracted the estimated total intracranial, total brain, gray matter, white matter, basal ganglia (caudate, putamen, pallidum, nucleus accumbens), and thalamus volumes. We normalized all volumes to the estimated total intracranial volume. We averaged the basal ganglia and thalamus volumes across the hemispheres. First, we tested a potential effect of scanner type and group x scanner type interaction using a general linear model (GLM) (dependent variable: normalized volume). There was no effect of scanner type or group x scanner interaction regarding any of the dependent variables. We used a separate GLM (dependent variable: normalized volume, fixed factor: group with three levels, covariate: age) to examine any group difference. For post hoc pairwise comparisons, we used the Tukey's HSD test when error variances were equal (Levene's test, $p > 0.05$) and the Games-Howell test when they were unequal. We set the statistical significance threshold for five pairwise comparisons of the subcortical structures at $p < 0.01$ (0.05/5). We performed the statistical analyses using SPSS 26.

Statistical analysis of cortical surfaces

We assessed the between-group differences in cortical thickness using the mri_glmfit function (with the "different offset different slope" option) in FreeSurfer. This function allowed a GLM analysis as described in the previous section. The smoothed cortical surfaces from both hemispheres using a Gaussian kernel with full width half maximum of 15 mm of all participants were the dependent variable and entered into a GLM first to test a potential effect of scanner type and group x scanner interaction. There was no effect of scanner type or group x scanner interaction regarding cortical thickness. We used a separate GLM (dependent variable: cortical thickness, fixed factor: group with three levels, covariate: age) to examine any group difference. We performed correction for multiple comparisons using the mri_glmfit-sim function, which performs Monte Carlo simulations. We set the significance threshold at 1.3 corresponding to $p < 0.05$.

SWI analysis

The SWI scan of each WD participant was inspected for subcortical hypointense lesions by a neurologist (A.V.R.) who was blinded to the subgroup assignment of the scans. We then tallied up the number of subjects and of brain structures with these hypointense lesions per WD subgroup.

DTI analysis

We averaged two separate diffusion image acquisitions and used the average to compute the diffusion tensors. We masked the individual subject tensors outside the brain and calculated the mean diffusivity (MD) and fractional anisotropy (FA) values from the tensor data. We spatially smoothed the FA maps with a 6-mm Gaussian kernel and nonlinearly registered them to the standard brain template JHU ICBM FA 2 mm (https://neurovault.org/images/1406/; Hua et al. 2008; Wakana et al. 2007). We demonstrated previously that registration using FA maps provides a better fit than does registration using the raw DTI data (Papademetris et al. 2001). We used two-sample t-tests to compare the differences in the FA maps between the WDH and WDN groups. We performed all analyses using the Yale BioImage Suite software package (Papademetris et al. 2006) following previously described techniques (Constable et al. 2008). To correct for multiple comparisons, we used family-wise error rate (FWE) correction determined by Monte Carlo simulation using the AFNI 3dClustSim program ($p < 0.02$).

Rs-fMRI analysis

We used the Connectivity toolbox for the rs-fMRI analysis (Whitfield-Gabrieli and Nieto-Castanon 2012). We concatenated the consecutive rs-fMRI scans. Preprocessing steps included the removal of the first four scans, motion correction, outlier detection, coregistration of functional scans with the anatomical scan, normalization to the standard Montreal Neurological Institute (MNI) brain template, and smoothing with an 8-mm kernel to account for inter-individual anatomical variability. Denoising steps included correction for physiological and other sources of noise by regressing out the principal components of the white matter and cerebrospinal fluid signal using the CompCor method (Chai et al. 2012), regression of motion artifacts and outliers before bandpass-filtering, and quadratic detrending. Global signal was not removed. Finally, we bandpass-filtered ($0.008 < f < 0.1$ Hz) the data to capture the resting-state fluctuations of the blood oxygenation level-dependent (BOLD) signal. The voxel-wise global mean correlations after denoising were compared between subjects across groups and scanners. We excluded subjects with maximum head motion exceeding the size of one-and-a-half voxels.

We used the functionally defined nodes ($n = 268$) in the whole-brain Shen Atlas for the FC analyses (Shen et al., 2013). For each subject, we extracted the BOLD signal time courses from these nodes and correlated them with each other using Pearson correlations. We Fisher z-transformed the correlations and obtained group-level FC maps for statistical analyses. First, we performed a one-way ANOVA with three groups to test for any group difference in FC. We then performed three post hoc pairwise group comparisons (i.e., WDH vs Control, WDN vs Control, and WDH vs WDN) using age as a covariate of no interest. We used the false discovery rate (FDR) method for correction for multiple comparisons (Genovese et al. 2002). We set the significance threshold at $p < 0.05$ for the ANOVA and at $p < 0.0167$ (0.05/3) for post hoc tests.

Post hoc correlation analyses

We performed separate correlation analyses between the UWDRS III scores of the WDN group and 1) normalized subcortical volumetric and mean FA values in SPSS 26, 2) cortical thickness values in FreeSurfer using the mri_glmfit function, and 3) rs-fMRI pairwise connectivity values in Connectivity toolbox ($p < 0.05$ for all regression models).

Results

Demographic and clinical data

The mean age ± standard deviation was 37.3 ± 10.1 years for the control group. Age did not differ significantly between the control, WDN, and WDH groups (one-way ANOVA, $F(2, 57) = 1.205$, $p = 0.307$). All participants were right-handed. Table 1 summarizes the characteristics of the WDN and WDH groups. Most common neurological exam findings in the WDN group were tremor (in 81% of subjects), dystonia (in 81% of subjects), and parkinsonism (in 69% of subjects). The RBANS, TMT-A/B, and fluency scores of both WDN and WDH groups were not significantly different from normative scores (Randolph et al. 1998; Tombaugh 2004; Tombaugh et al. 1999). Five participants in the WDN and seven in the WDH group were asymptomatic at the time of diagnosis and were diagnosed on the basis of abnormal liver function tests or family screening. Five participants in each group had liver cirrhosis. All participants in the WD group were on chronic treatment for at least one year (exact duration was unknown for one participant in each group). The duration and type of treatment did not differ between the WDN and WDH groups and had the following distribution: WDN: penicillamine ($n = 1$), trientine ($n = 3$), tetrathiomolybdate ($n = 2$), zinc ($n = 10$); WDH: penicillamine ($n = 1$), trientine ($n = 5$), tetrathiomolybdate ($n = 2$), zinc ($n = 5$), and combination of trientine and zinc ($n = 1$).

Imaging data

There was no evidence for brain infarction, intracranial hemorrhage, mass effect, or edema on T1- and T2-weighted images.

Subcortical volumes

Table S1 in Supplementary Material shows the raw segmented volumes. There was a significant group effect in white matter, caudate, putamen, and thalamic volumes. There was no group-by-age interaction in any of the volumes. The subcortical atrophy was driven by the WDN group. Both WDN and WDH showed significantly reduced white matter volumes compared to controls (Table 2).

SWI

Fifteen participants in the WDN and four in the WDH group had hypointense lesions in the basal ganglia and red nucleus on the SWI scans ($p = 0.000$) (Supplementary Material Table S2).

Cortical thickness

The GLM analysis did not reveal a significant WD subgroup effect. The post hoc analysis using the WD group as a whole compared to controls showed significant cortical thinning in bilateral superior frontal cortex (Fig. 1, top panel).

Table 1 Demographics and neuropsychiatric profiles of WDN and WDH subgroups.

		WDN ($N = 16$)	WDH ($N = 14$)	p value
Age (years)		43.1 ± 14.7	38.4 ± 12.9	0.553
Gender	Male	6	7	0.491
	Female	10	7	
Ethnicity	Caucasian	16	13	0.277
	Non-Caucasian	0	1	
Education	Secondary	2	0	0.121
	College	10	6	
	Graduate/Professional	4	8	
Age at diagnosis (years)		22.0 ± 15.5^	25.1 ± 16.7	0.508
Age at symptom onset (years)		23.5 ± 15.4†	28.3 ± 11.4‡	0.457
Treatment duration (years)		21.3 ± 16.5	15.4 ± 15.7	0.254
Treatment at enrollment	Chelation	6	9	0.143
	Zinc	10	6	
Kayser-Fleischer rings	Present at diagnosis	9	3	0.035
	Unknown	1	0	
UWDRS II		3.5 ± 5.5	0.6 ± 2.4	0.085
UWDRS III		16.2 ± 17.5	0.0 ± 0.0	0.000
DSM-5 CCM		13.3 ± 13.3	8.1 ± 10.7	0.294
RBANS total		100.9 ± 13.3*	106.1 ± 11.6	0.272
Executive Function	TMT-A	32.3 ± 8.2**	28.6 ± 6.9	0.203
	TMT-B	63.8 ± 18.3**	56.0 ± 12.1	0.172
	Fluency	12.9 ± 2.8*	14.0 ± 3.4	0.336

Mean ± standard deviation. DSM-5 CCM: Diagnostic Statistical Manual 5 Self-Rated Level 1 Cross-Cutting Symptom Measure, RBANS: Repeated Battery for Assessment of Neuropsychological Status composite score of all domains converted to an age-corrected standard score (mean = 100; SD = 15), TMT: Trail making test, UWDRS: Unified Wilson Disease Rating Scale, WDH/N: Wilson disease hepatic/neurologic group

^: Unknown age of diagnosis in one participant. †WDN ($N = 11$), ‡WDH ($N = 7$). *WDN (N = 14) and **WDN ($N = 15$): Two participants could not complete the RBANS and phonemic fluency test due to severe dysarthria and difficulty holding a pen. One of these participants was also unable to perform the TMT

DSM-5 CCM, TMT-B, UWDRS III scores, and treatment duration were not normally distributed. The p values for these variables reflect the results of Mann Whitney U tests

DTI

We excluded the DTI data of one subject in the WDN group due to excessive head motion. There was no significant difference between the WDH and WDN groups in the mean whole-brain MD and FA values ($p = 0.100$ and 0.750, respectively. WDH: MD: 1.17 ± 0.09 and FA: 0.22 ± 0.02; WDN: MD: 1.23 ± 0.12, FA: 0.21 ± 0.02). The WDH group showed

Table 2 WDH ($n = 14$) vs WDN ($n = 16$) vs Control ($n = 30$) Volumetric Comparisons

Volume	F (2, 56)	P value	Significant pairwise comparisons (p value)
Total brain	2.042	0.118	–
Total GM	3.991	0.012	–
Cerebral WM	5.448	0.002	WDN vs control (0.004) and WDH vs control (0.009)
Caudate	11.006	0.000	WDN vs control (0.000) and WDN vs WDH (0.000)
Putamen	12.263	0.000	WDN vs control (0.003) and WDN vs WDH (0.004)*
Pallidum	1.502	0.224	–
Accumbens	6.219	0.001	WDN vs control (0.015) and WDN vs WDH (0.031)*^
Thalamus	3.853	0.014	WDN vs control (0.005)

*Levene's test was significant ($p < 0.05$) and Games-Howell test was used for post hoc comparisons. ^: This should be interpreted as trend. GM: Gray matter, WDH/N: Wilson disease hepatic/neurologic group, WM: White matter

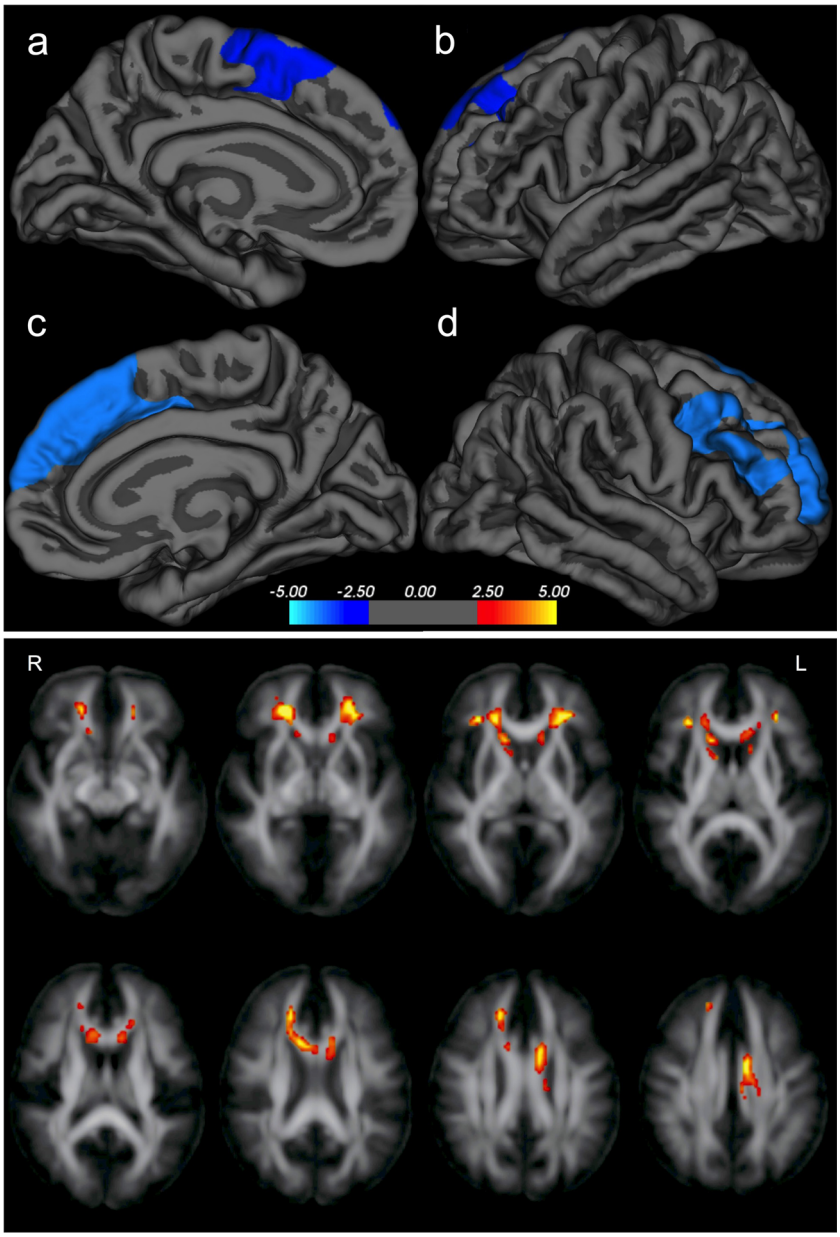

Fig. 1 *Top panel*: Cortical thinning in WD compared to controls in (a) left medial and (b) left lateral superior frontal cortex (MNI coordinates: x = −20, y = 32, z = 32, Brodmann area (BA) 8 extending to BA 6, maximum: −2.96, cluster size = 2403 mm^2), (c) right medial and (d) right lateral superior frontal cortex (MNI coordinates: x = 37, y = 7, z = 36, BA 8, extending to BA 9, maximum: −3.19, cluster size = 6016 mm^2). Color bar displays the Monte Carlo significance thresholds. *Bottom panel*: Higher fractional anisotropy in WDN < WDH in the genu and body of the corpus callosum, and in bilateral anterior corona radiata bundles (FWE-corrected $p = 0.02$, t = 2.472, cluster size = 192 voxels)

significantly higher FA compared to the WDN group in the genu and body of the corpus callosum, and in bilateral anterior corona radiata bundles (Fig. 1, bottom panel).

Rs-fMRI

We excluded six subjects from the WD (2 WDN, 4 WDH) and six from the control group due to excessive head motion. There was no significant between-group difference in head motion in the included subjects (Supplementary Material Table S3). There were no group or scanner differences in global voxel-wise correlations (Supplementary Material) suggesting that potential scanner effects were removed after denoising. The ANOVA revealed group differences in the FC between hundreds of node pairs. In post hoc analyses, WDH compared to controls showed predominantly increased FC especially between the left hippocampus and occipito-temporal nodes and between the right superior frontal sulcus and fronto-parietal nodes (Fig. 2, Table 3). WDN compared to controls showed predominantly decreased FC especially between bilateral caudate and fronto-parietal and cerebellar nodes (Fig. 2, Table 3). Increased FC specifically between the left premotor and occipital nodes was common in both WDH and WDN groups compared to controls. WDH compared to WDN demonstrated increased FC only between the right supramarginal and temporal pole nodes.

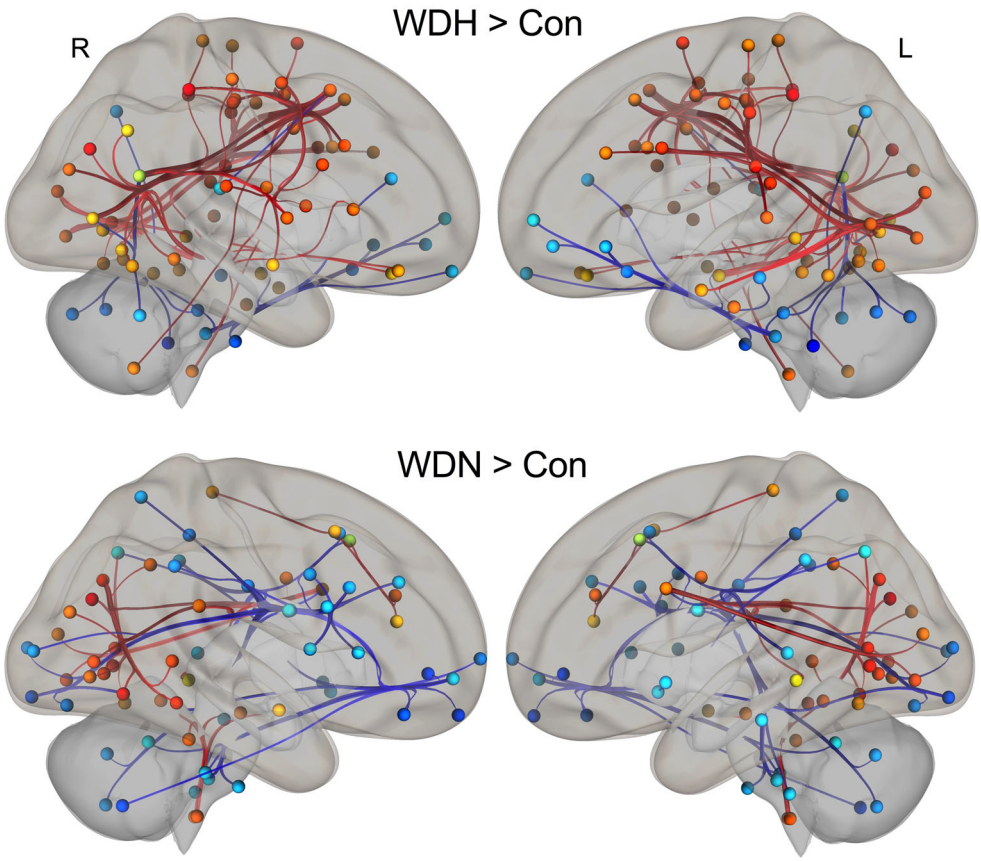

Fig. 2 Pairwise nodal functional connectivity differences (cool colors: decreased, warm colors: increased) between WDH > Control and WDN > Control displayed on the right (R) and left (L) hemispheres of the MNI template. See Table 3 and the interactive webpage https://bioimagesuiteweb.github.io/webapp/connviewer.html for the coordinates of the Shen Atlas nodes

Post hoc correlations

We observed no significant correlations between the UWDRS III scores and any of the structural measures in the WDN group. The UWDRS III scores showed significant negative correlations with the FC mainly between the inferior frontal node and cerebellar and occipital nodes (Supplementary Material Fig. S1, Table S4).

Discussion

In summary, our results demonstrate the presence of diffuse white matter atrophy and altered functional brain organization even in neurologically non-manifesting WD patients. The structural and functional brain changes are more prominent in the neurologically manifesting WD patients and strongly involve the basal ganglia.

Our structural findings are in line with prior reports in the literature demonstrating volume loss (Sinha et al. 2007; Stezin et al. 2016; Zou et al. 2019) and MRI signal abnormalities (Fritzsch et al. 2014; Kozić et al. 2003; Litwin et al. 2013; Südmeyer et al. 2006; Yang et al. 2015) in the basal ganglia in patients with WD. Diffuse atrophy in white matter and cortical gray matter has also been reported in WD (Sinha et al. 2007; Stezin et al. 2016) and was found to correlate with neurological impairment (Smolinski et al. 2019).

We carefully characterized the WDH and WDN phenotypes based on neurological signs and matched their demographic, treatment, and psychiatric profiles. As expected, many of the observed structural brain differences especially in the subcortical regions were driven mainly by the WDN group. The WDN group also had significantly more SWI hypointensities in subcortical structures compared to the WDH group. Yet, it is important to note that the WDH group also showed significant white matter volume loss compared to controls. In the brain, copper toxicity first leads to reactive astrogliosis, which serves to buffer excess copper, and eventually to astrocytic damage, demyelination, and neuronal death (Członkowska et al. 2018; Pal and Prasad 2014). In a MRI study, copper overload was found to correlate with lower total brain, white matter, and gray matter volumes in drug-naïve patients with WD (Smolinski et al. 2019). Notably, a number of hepatic diseases with varying etiologies may have neurological manifestations and corresponding structural brain changes. For example, primary biliary cholangitis (PBC), an autoimmune liver disease, may present with neurological symptoms. Non-cirrhotic patients with PBC compared to matched controls show reduced thalamic volume (Mosher et al. 2019). Hepatic encephalopathy is associated with

Table 3 Pairwise nodal functional connectivity differences

WDH > Control

Increased Connectivity

Node Pairs	*Pair Labels*			
Numbers	**Node 1 (BA)**	**Node 2 (BA)**	**T(32)**	**p-FDR**
(230)-(190)	L hippocampus (BA54)	L MTG (BA21)	6.06	0.0003
(204)–(22)	L VA (BA19)	R IFG (BA44)	5.45	0.0011
(22)–(210)	R IFG (BA44)	L V2 (BA18)	5.32	0.0011
(204)–(157)	L VA (BA19)	L PMC (BA6)	4.96	0.0032
(231)–(204)	L hippocampus (BA54)	L VA (BA19)	4.80	0.0034
(231)–(68)	L hippocampus (BA54)	R FG (BA37)	4.88	0.0035
(231)–(207)	L hippocampus (BA54)	L VA (BA19)	4.79	0.0035
(231)–(209)	L hippocampus (BA54)	L VA (BA19)	4.62	0.0037
(231)–(206)	L hippocampus (BA54)	L VA (BA19)	4.59	0.0037
(22)–(73)	R IFG (BA44)	R VA (BA19)	4.77	0.0037
(210)–(157)	L V2 (BA18)	L PMC (BA6)	4.80	0.0052
(266)–(20)	L brainstem	R IFG (BA45)	4.99	0.0059
(231)–(68)	L hippocampus (BA54)	R FG (BA37)	4.88	0.0082
(209)–(196)	L VA (BA19)	L ITG (BA20)	4.64	0.0086
(230)–(48)	L hippocampus (BA54)	R AG (BA39)	4.60	0.0091
(209)–(17)	L VA (BA19)	R IFG (BA47)	4.45	0.0092
(231)–(211)	L hippocampus (BA54)	L V2 (BA18)	4.08	0.0096
(231)–(200)	L hippocampus (BA54)	L FG (BA37)	4.05	0.0096
(231)–(210)	L hippocampus (BA54)	L V2 (BA18)	4.04	0.0096
(157)–(73)	L PMC (BA6)	R VA (BA19)	4.40	0.0106
(209)–(171)	L VA (BA19)	L S1 (BA1)	4.29	0.0108
(30)–(61)	R SFS (BA8)	R STG (BA41)	4.37	0.0123
(30)–(171)	R SFS (BA8)	L S1 (BA1)	4.03	0.0123
(30)–(89)	R SFS (BA8)	R PCC (BA31)	4.02	0.0123
(30)–(191)	R SFS (BA8)	L MTG (BA21)	3.99	0.0123
(30)–(221)	R SFS (BA8)	L ACC (BA24)	3.99	0.0123
(30)–(32)	R SFS (BA8)	R PMC (BA6)	3.98	0.0123
(30)–(162)	R SFS (BA8)	L SMA (BA6)	3.93	0.0123
(30)–(209)	R SFS (BA8)	L VA (BA19)	3.92	0.0123
(30)–(35)	R SFS (BA8)	R Insula (BA13)	3.91	0.0123
(30)–(181)	R SFS (BA8)	L SMG (BA40)	3.86	0.0123
(30)–(218)	R SFS (BA8)	L PCC (BA31)	3.85	0.0123
(30)–(33)	R SFS (BA8)	R S1 (BA1)	3.83	0.0123
(30)–(167)	R SFS (BA8)	L S1 (BA1)	3.79	0.0123
(30)–(179)	R SFS (BA8)	L SMG (BA40)	3.78	0.0123
(30)–(161)	R SFS (BA8)	L ACC (BA24)	3.77	0.0123
(231)–(198)	L hippocampus (BA54)	L FG (BA37)	3.88	0.0125
(231)–(66)	L hippocampus (BA54)	R FG (BA37)	3.84	0.0126
(86)–(62)	R PCC (BA23)	R STG (BA41)	4.33	0.0129
(230)–(64)	L hippocampus (BA54)	R STG (BA22)	4.33	0.0130
(157)–(74)	L PMC (BA6)	R VA (BA19)	4.21	0.0136
(230)–(3)	L hippocampus (BA54)	R OFC (BA11)	4.21	0.0137
(150)–(38)	L SFG (BA8)	R S1 (BA1)	4.48	0.0138
(150)–(266)	L SFG (BA8)	L brainstem	4.25	0.0138
(150)–(210)	L SFG (BA8)	L V2 (BA18)	4.20	0.0138
(86)–(191)	R PCC (BA23)	L MTG (BA21)	4.05	0.0145

Table 3 (continued)

(86)–(84)	R PCC (BA23)	R ACC (BA24)	3.99	0.0145
(171)–(49)	L S1 (BA1)	R AG (BA39)	4.67	0.0149
(30)–(38)	R SFS (BA8)	R S1 (BA1)	3.65	0.0151
(231)–(72)	L hippocampus (BA54)	R VA (BA19)	3.74	0.0155
(30)–(109)	R SFS (BA8)	R cerebellum	3.60	0.0162
Decreased Connectivity				
Node Pairs	*Pair Labels*			
Numbers	**Node 1 (BA)**	**Node 2 (BA)**	**T(32)**	**p-FDR**
(86)–(253)	R PCC (BA23)	L cerebellum	−5.53	0.0007
(86)–(252)	R PCC (BA23)	L cerebellum	−5.50	0.0007
(131)–(153)	R brainstem	L IFG (BA47)	−5.66	0.0009
(231)–(83)	L hippocampus (BA54)	R ACC (BA32)	−4.51	0.0039
(267)–(1)	L brainstem	R OFC (BA11)	−4.44	0.0142
(267)–(143)	L brainstem	L FP (BA10)	−4.42	0.0142
(267)–(151)	L brainstem	L IFG (BA47)	−4.20	0.0142
(267)–(153)	L brainstem	L IFG (BA47)	−4.19	0.0142
(86)–(247)	R PCC (BA23)	L cerebellum	−4.00	0.0145
(267)–(182)	L brainstem	L AG (BA39)	−4.00	0.0148
(267)–(193)	L brainstem	L MTG (BA21)	−3.99	0.0148
(267)–(142)	L brainstem	L FP (BA10)	−3.98	0.0148
(74)–(245)	R VA (BA19)	L cerebellum	−4.32	0.0150
(30)–(127)	R SFS (BA8)	R thalamus	−3.65	0.0151
(86)–(113)	R PCC (BA23)	R cerebellum	−3.92	0.0151
WDN > Control				
Increased Connectivity				
Node Pairs	*Pair Labels*			
Numbers	**Node 1 (BA)**	**Node 2 (BA)**	**T(35)**	**p-FDR**
(157)–(74)	L PMC (BA6)	R VA (BA19)	5.75	0.0004
(157)–(73)	L PMC (BA6)	R VA (BA19)	5.49	0.0005
(157)–(210)	L PMC (BA6)	L V2 (BA18)	5.30	0.0006
(225)–(220)	L PCC (BA31)	L ACC (BA24)	5.12	0.0029
(157)–(209)	L PMC (BA6)	L VA (BA19)	4.63	0.0032
(176)–(72)	L precuneus (BA7)	R VA (BA19)	5.09	0.0033
(157)–(204)	L PMC (BA6)	L VA (BA19)	4.37	0.0056
(244)–(129)	L cerebellum	R brainstem	4.81	0.0077
(266)–(265)	L brainstem	L brainstem	4.49	0.0080
(266)–(99)	L brainstem	R hippocampus (BA54)	4.42	0.0080
(266)–(244)	L brainstem	L cerebellum	4.38	0.0080
(266)–(103)	L brainstem	R cerebellum	4.33	0.0080
(176)–(68)	L precuneus (BA7)	R FG (BA37)	4.39	0.0122
(157)–(207)	L PMC (BA6)	L VA (BA19)	4.03	0.0123
(122)–(230)	R caudate	L hippocampus (BA54)	4.02	0.0133
(182)–(98)	L AG (BA39)	R V2 (BA18)	4.37	0.0140
(30)–(172)	R SFS (BA8)	L S1 (BA1)	4.36	0.0157
(30)–(83)	R SFS (BA8)	R ACC (BA32)	4.33	0.0157
Decreased Connectivity				
Node Pairs	*Pair Labels*			
Numbers	**Node 1 (BA)**	**Node 2 (BA)**	**T(35)**	**p-FDR**
(150)–(229)	L SFG (BA8)	L hippocampus (BA54)	−5.02	0.0020
(88)–(212)	L PCC (BA23)	L V2 (BA18)	−4.82	0.0026
(88)–(213)	L PCC (BA23)	L V2 (BA18)	−4.82	0.0026
(88)–(214)	L PCC (BA23)	L V2 (BA18)	−4.81	0.0026
(182)–(17)	L AG (BA39)	R IFG (BA47)	−4.99	0.0044
(260)–(20)	L caudate	R IFG (BA45)	−4.85	0.0068
(131)–(193)	R brainstem	L MTG (BA21)	−4.81	0.0077
(214)–(5)	L V2 (BA18)	R FP (BA10)	−4.54	0.0084
(259)–(169)	L caudate	L insula (BA13)	−4.77	0.0085
(260)–(35)	L caudate	R Insula (BA13)	−4.36	0.0093
(260)–(22)	L caudate	R IFG (BA44)	−4.31	0.0093
(260)–(184)	L caudate	L AG (BA39)	−4.24	0.0093
(260)–(21)	L caudate	R IFG (BA44)	−4.20	0.0093
(260)–(133)	L caudate	R brainstem	−4.05	0.0108
(88)–(6)	L PCC (BA23)	R FP (BA10)	−4.22	0.0111
(157)–(229)	L PMC (BA6)	L hippocampus (BA54)	−3.99	0.0123

Table 3 (continued)

(7)–(267)	R FP (BA10)	L brainstem	−4.47	0.0127
(7)–(255)	R FP (BA10)	L cerebellum	−4.28	0.0127
(7)–(116)	R FP (BA10)	R cerebellum	−4.27	0.0127
(122)–(47)	R caudate	R SMG (BA40)	−4.53	0.0133
(122)–(133)	R caudate	R brainstem	−4.38	0.0133
(122)–(22)	R caudate	R IFG (BA44)	−4.20	0.0133
(122)–(256)	R caudate	L cerebellum	−3.94	0.0133
(122)–(44)	R caudate	R precuneus (BA7)	−3.91	0.0133
(122)–(35)	R caudate	R insula (BA13)	−3.90	0.0133
(122)–(253)	R caudate	L cerebellum	−3.87	0.0133
(122)–(91)	R caudate	R PCC (BA31)	−3.83	0.0138
(122)–(240)	R caudate	L cerebellum	−3.77	0.0139
(122)–(11)	R caudate	R SFG (BA9)	−3.76	0.0139
(122)–(31)	R caudate	R PMC (BA6)	−3.70	0.0145
(122)–(184)	R caudate	L AG (BA39)	−3.69	0.0145
(214)–(1)	L V2 (BA18)	R OFC (BA11)	−4.20	0.0156
(267)–(193)	L brainstem	L MTG (BA21)	−4.32	0.0164
(260)–(17)	L caudate	R IFG (BA47)	−3.83	0.0165
(260)–(28)	L caudate	R SMA (BA6)	−3.80	0.0165
WDH > WDN				
Increased Connectivity				
Node Pairs	*Pair Labels*			
Numbers	**Node 1 (BA)**	**Node 2 (BA)**	**T(21)**	**p-FDR**
(47)–(51)	R SMG (BA40)	R TP (BA38)	5.32	0.0075

The numbers refer to the node numbers in the Shen Atlas. See the interactive webpage https://bioimagesuiteweb.github.io/webapp/connviewer.html for the coordinates of the nodes. The significance threshold was set at FDR-corrected $p < 0.0167$

ACC: Anterior cingulate cortex, AG: Angular gyrus, BA: Brodmann area, FG: Fusiform gyrus, FP: Frontal pole, IFG: Inferior frontal gyrus, ITG: Inferior temporal gyrus, MTG: Middle temporal gyrus, OFC: Orbitofrontal cortex, PCC: Posterior cingulate cortex, PMC: Premotor cortex, S1: Primary somatosensory cortex, SFG: Superior frontal gyrus, SFS: Superior frontal sulcus, SMA: Supplementary motor area, SMG: Supramarginal gyrus, STG: Superior temporal gyrus, TP: Temporal pole, V2: Secondary visual area, VA: Visual association area, WDH/N: Wilson disease hepatic/neurologic group

Note: Nodes 131/133/267 and 129/266 correspond to pons and medulla, respectively

indirect astrocyte degeneration, which is observed as specific MRI signal abnormalities in the basal ganglia (Hermann 2014). Cirrhotic patients (alcohol and/or viral etiology) show decreased gray matter volume in the basal ganglia, thalamus, and cerebellum as well as many cortical regions compared to matched controls (García-García et al. 2017). These changes are more prominent in those with minimal hepatic encephalopathy (MHE).

None of our subjects had known portosystemic shunting or encephalopathy, or a history of alcohol abuse or viral hepatitis based on history and clinical examination and laboratory testing. Therefore, the most plausible explanation for the insidious, subclinical white matter damage in the WDH group in our study is direct copper toxicity. MRI with volumetric analysis can be helpful in detecting this damage.

Cortical lesions are thought to be rare in treated patients with WD (Magalhaes et al. 1994; Prashanth et al. 2005). Interestingly, we found significant regional thinning in the superior frontal cortex in the WD whole group compared to controls. All of our subjects were on chronic treatment for their WD and did not have a history of any other neurological disease to explain the cortical atrophy. Direct cortical neuronal damage due to copper toxicity may be one of the reasons underlying the cortical thinning. Alternatively, white matter loss may have caused retrograde degeneration in the cortical neurons. Our DTI findings lend partial support to this hypothesis. Lack of DTI data from the control group precluded a comparison between the WD and control groups. However, we did find loss of integrity in specific white matter tracts including the corpus callosum and bilateral anterior corona radiata in the WDN compared to the WDH group. The anterior corona radiata carries the white matter bundles that connect the frontal cortex with the thalamus, basal ganglia, and brainstem. These bundles cross between the two hemispheres in the genu of the corpus callosum (Bruni and Montemurro 2009). Damage to these tracts would be expected to lead to regional atrophy in the frontal cortex via retrograde degeneration. Regional changes in white matter integrity have also been reported in the frontal and occipital lobes, bilateral internal capsule, and midbrain and pons in drug-naïve patients with WD (Jadav et al. 2013).

The alterations in the functional brain organization were also differentially expressed in the WDN and WDH groups compared to controls. As hypothesized, we found a robust decrease in the frontal cortex-basal ganglia (caudate) FC, but only in the WDN group. This is consistent with previous

findings (Jing et al. 2019). The caudate also showed reduced FC with parietal and cerebellar nodes in the WDN group compared to controls. Notably, neurological disease severity negatively correlated with the inferior frontal-cerebellar FC in the WDN group consistent with previous reports of cerebellar dysfunction in WD (Hu et al. 2017; Jing et al. 2019). Tremor and dystonia were also most common neurological manifestations in our WDN group, both of which are associated with cerebellar dysfunction (Bareš et al. 2019). The FC alterations in the WDH group displayed a different pattern. Specifically, the diffusely increased hippocampal FC in the WDH compared to the control group was unexpected and its neurobiological significance is elusive. Reduced hippocampal FC has been reported in cirrhotic patients with MHE compared to those without MHE and controls (García-García et al. 2018; Lin et al. 2019). On the other hand, non-cirrhotic patients with PBC compared to controls were found to have increased hippocampal FC with the putamen, thalamus, and frontotemporal regions, which was also associated with treatment response (Mosher et al. 2017). Increased astrocytosis in the hippocampus has been shown in rodent models of copper toxicity (Kalita et al. 2018; Terwel et al. 2011). Interestingly, in a mouse model of WD, despite astrocytosis, hippocampal synapses were structurally intact, in fact, the level of presynaptic marker synaptophysin was slightly increased, perhaps reflecting a compensatory mechanism (Terwel et al. 2011). These findings suggest that copper deposition may impair synaptic transmission in the hippocampus leading to abnormal FC. Finally, both WDH and WDN compared to controls showed increased FC of the premotor/superior frontal nodes. The location of these nodes overlaps with that of the cortical thinning suggesting that changes in regional cortical architecture result in aberrant FC.

Our findings may also have prognostic and management implications. While it is generally accepted that once WD is diagnosed treatment must be initiated, optimal strategies for treatment and outcome monitoring are lacking. Though treatment can prevent the progression of neurologic disease, some individuals with advanced disease may have irreversible changes. In a longitudinal study, anti-copper treatment was found to be effective in improving the clinical and radiographic profile (e.g., atrophy, focal lesions) in 71% of 50 patients with WD. Patients with extensive white matter involvement and severe diffuse atrophy demonstrated a poor prognosis despite treatment (Sinha et al. 2007). Reliable structural imaging parameters may better identify those most likely to benefit from treatment. The treatment of WD patients with neurological signs remains a source of uncertainty, as copper chelation is known to worsen neurological function in some drug-naïve patients, sometimes irrevocably. Early neurological worsening with anti-copper treatment was observed in 11.1% of 143 patients involving only those who had neurological signs at diagnosis, and was associated with a higher prevalence of thalamic and brainstem lesions on MRI (Litwin et al. 2015). A recent study measured the acute toxicity and chronic damage in the brain in WD patients with WDN and WDH subgroups at baseline and after two years of anti-copper treatment using different MRI sequences and a visual MRI rating scale. A significant correlation was found only between chronic damage (driven by the brain atrophy scores) and UWDRS III scores in the WDN subgroup at baseline and follow-up. Consistent with previous reports, one WDN patient whose neurological condition worsened after treatment also developed extensive white matter lesions (Dusek et al. 2020). All of these reports emphasize the role of brain MRI assessments in monitoring the treatment response in WD. Here, we further highlight this role by demonstrating detailed quantitative assessments of brain atrophy not only in WDN but also in WDH using readily available and fully automated segmentation methods.

We think that our findings have critical implications for clinical trials and therapeutic considerations in WD. Our study along with others in the literature suggests that perhaps brain involvement is inevitable and should be expected at any stage in WD as our observation of white matter atrophy in the WDH group indicates. Therefore, in addition to the clinical characterization of the hepatic and neurological WD phenotypes, it may be important to obtain a baseline T1-weighted MRI (e.g., MPRAGE) scan of the brain for volumetric analysis before the initiation of treatment. We would further suggest repeating these scans and analyses (e.g., annually) along with longitudinal clinical follow-up. These scans could potentially be used as a biomarker to aid in predicting phenotype conversion and prognosis for achieving further improvement, and assist with the monitoring of treatment response. The cross-sectional nature of our study and the relatively small size of our WD cohort are limitations that prevent us from making longitudinal predictions based on our imaging data. Therefore, further study of brain imaging in WD at the start of and during the course of treatment may help determine longitudinal imaging parameters in this disease, and help establish brain imaging as a useful biomarker for WD.

Conclusions

Our cross-sectional study shows structural and functional brain changes even in neurologically non-manifesting WD patients. These findings imply that longitudinal brain MRI scans combined with quantitative volumetric analyses may be valuable for further prognostic assessments and optimization of treatment strategies in WD.

Supplementary Information The online version contains supplementary material available at https://doi.org/10.1007/s11682-020-00420-5.

Acknowledgments We thank the Wilson Disease Association for their help with participant recruitment.

Availability of data and material Not applicable.

Code availability Not applicable.

Authors' contributions Study conceptualization and design: ST, DR, MLS, RTC. Data collection: KN, AVR, JA. Data analysis and interpretation: ST, JA, KN, AVR, MS, AP, RTC. Supervision of the study procedures: ST, DR, RTC, MLS. Drafting the manuscript: ST. All authors contributed to the final version of the manuscript.

Funding This study was supported through the grants from the Jack Levin Foundation, The Rachel and Drew Katz Foundation and the Albert Family to the Yale University School of Medicine.

Compliance with ethical standards

Conflict of interest Authors Tinaz, Arora, Nalamada, Vives-Rodriguez, Sezgin, Robakis, Patel, and Constable declare that they have no conflict of interest. Author Schilsky received grant funding from Alexion and GMPO.

Ethical approval All procedures were in accordance with the ethical standards of the institutional and/or national research committee and with the 1964 Helsinki declaration and its later amendments or comparable ethical standards.

Consent to participate Informed consent was obtained from all participants included in the study.

Consent for publication Not applicable.

References

Bareš, M., Apps, R., Avanzino, L., Breska, A., D'Angelo, E., Filip, P., Gerwig, M., Ivry, R. B., Lawrenson, C. L., Louis, E. D., Lusk, N. A., Manto, M., Meck, W. H., Mitoma, H., & Petter, E. A. (2019). Consensus paper: Decoding the contributions of the cerebellum as a time machine. From neurons to clinical applications. *Cerebellum (London, England), 18*(2), 266–286. https://doi.org/10.1007/s12311-018-0979-5.

Bennett, J., & Hahn, S. H. (2011). Clinical molecular diagnosis of Wilson disease. *Seminars in Liver Disease, 31*(3), 233–238. https://doi.org/10.1055/s-0031-1286054.

Bruni, J. E., & Montemurro, D. G. (2009). *Human Neuroanatomy: A text, brain atlas, and laboratory dissection guide* (3rd ed.). New York: Oxford University Press.

Chai, X. J., Castañón, A. N., Ongür, D., & Whitfield-Gabrieli, S. (2012). Anticorrelations in resting state networks without global signal regression. *NeuroImage, 59*(2), 1420–1428. https://doi.org/10.1016/j.neuroimage.2011.08.048.

Clarke, D. E., & Kuhl, E. A. (2014). DSM-5 cross-cutting symptom measures: A step towards the future of psychiatric care? *World psychiatry : official journal of the World Psychiatric Association (WPA), 13*(3), 314–316. https://doi.org/10.1002/wps.20154.

Conn, H. O. (1977). Trailmaking and number-connection tests in the assessment of mental state in portal systemic encephalopathy. *The American Journal of Digestive Diseases, 22*(6), 541–550. https://doi.org/10.1007/BF01072510.

Constable, R. T., Ment, L. R., Vohr, B. R., Kesler, S. R., Fulbright, R. K., Lacadie, C., Delancy, S., Katz, K. H., Schneider, K. C., Schafer, R. J., Makuch, R. W., & Reiss, A. R. (2008). Prematurely born children demonstrate white matter microstructural differences at 12 years of age, relative to term control subjects: An investigation of group and gender effects. *Pediatrics, 121*(2), 306–316. https://doi.org/10.1542/peds.2007-0414.

Członkowska, A., Litwin, T., Dusek, P., Ferenci, P., Lutsenko, S., Medici, V., Rybakowski, J. K., Weiss, K. H., & Schilsky, M. L. (2018). Wilson disease. *Nature reviews. Disease primers, 4*(1), 21. https://doi.org/10.1038/s41572-018-0018-3.

Członkowska, A., Tarnacka, B., Möller, J. C., Leinweber, B., Bandmann, O., Woimant, F., & Oertel, W. H. (2007). Unified Wilson's disease rating scale - a proposal for the neurological scoring of Wilson's disease patients. *Neurologia i Neurochirurgia Polska, 41*(1), 1–12.

Dale, A. M., Fischl, B., & Sereno, M. I. (1999). Cortical surface-based analysis. I. Segmentation and surface reconstruction. *NeuroImage, 9*(2), 179–194. https://doi.org/10.1006/nimg.1998.0395.

Dusek, P., Smolinski, L., Redzia-Ogrodnik, B., Golebiowski, M., Skowronska, M., Poujois, A., Laurencin, C., Jastrzebska-Kurkowska, I., Litwin, T., & Członkowska, A. (2020). Semiquantitative scale for assessing brain MRI abnormalities in Wilson disease: A validation study. *Movement disorders : official journal of the Movement Disorder Society, 35*(6), 994–1001. https://doi.org/10.1002/mds.28018.

Favrole, P., Chabriat, H., Guichard, J. P., & Woimant, F. (2006). Clinical correlates of cerebral water diffusion in Wilson disease. *Neurology, 66*(3), 384–389. https://doi.org/10.1212/01.wnl.0000196482.71636.7d.

Ferenci, P., Caca, K., Loudianos, G., Mieli-Vergani, G., Tanner, S., Sternlieb, I., Schilsky, M., Cox, D., & Berr, F. (2003). Diagnosis and phenotypic classification of Wilson disease. *Liver international: official journal of the International Association for the Study of the Liver, 23*(3), 139–142. https://doi.org/10.1034/j.1600-0676.2003.00824.x.

Fischl, B., & Dale, A. M. (2000). Measuring the thickness of the human cerebral cortex from magnetic resonance images. *Proceedings of the National Academy of Sciences of the United States of America, 97*(20), 11050–11055. https://doi.org/10.1073/pnas.200033797.

Fischl, B., Salat, D. H., Busa, E., Albert, M., Dieterich, M., Haselgrove, C., van der Kouwe, A., Killiany, R., Kennedy, D., Klaveness, S., Montillo, A., Makris, N., Rosen, B., & Dale, A. M. (2002). Whole brain segmentation: Automated labeling of neuroanatomical structures in the human brain. *Neuron, 33*(3), 341–355. https://doi.org/10.1016/s0896-6273(02)00569-x.

Fischl, B., Sereno, M. I., & Dale, A. M. (1999). Cortical surface-based analysis. II: Inflation, flattening, and a surface-based coordinate system. *NeuroImage, 9*(2), 195–207. https://doi.org/10.1006/nimg.1998.0396.

Fritzsch, D., Reiss-Zimmermann, M., Trampel, R., Turner, R., Hoffmann, K. T., & Schäfer, A. (2014). Seven-tesla magnetic resonance imaging in Wilson disease using quantitative susceptibility mapping for measurement of copper accumulation. *Investigative Radiology, 49*(5), 299–306. https://doi.org/10.1097/RLI.0000000000000010.

Gao, J., Brackley, S., & Mann, J. P. (2019). The global prevalence of Wilson disease from next- generation sequencing data. *Genetics in medicine : official journal of the American College of Medical Genetics, 21*(5), 1155–1163. https://doi.org/10.1038/s41436-018-0309-9.

García-García, R., Cruz-Gómez, Á. J., Mangas-Losada, A., Urios, A., Forn, C., Escudero-García, D., Kosenko, E., Ordoño, J. F., Tosca, J., Giner-Durán, R., Serra, M. A., Avila, C., Belloch, V., Felipo, V., & Montoliu, C. (2017). Reduced resting state connectivity and gray matter volume correlate with cognitive impairment in minimal

hepatic encephalopathy. *PLoS One, 12*(10), e0186463. https://doi.org/10.1371/journal.pone.0186463.

García-García, R., Cruz-Gómez, Á. J., Urios, A., Mangas-Losada, A., Forn, C., Escudero-García, D., Kosenko, E., Torregrosa, I., Tosca, J., Giner-Durán, R., Serra, M. A., Avila, C., Belloch, V., Felipo, V., & Montoliu, C. (2018). Learning and memory impairments in patients with minimal hepatic encephalopathy are associated with structural and functional connectivity alterations in Hippocampus. *Scientific Reports, 8*(1), 9664. https://doi.org/10.1038/s41598-018-27978-x.

Genovese, C. R., Lazar, N. A., & Nichols, T. (2002). Thresholding of statistical maps in functional neuroimaging using the false discovery rate. *NeuroImage, 15*(4), 870–878. https://doi.org/10.1006/nimg.2001.1037.

Han, Y., Cheng, H., Toledo, J. B., Wang, X., Li, B., Han, Y., Wang, K., & Fan, Y. (2016). Impaired functional default mode network in patients with mild neurological Wilson's disease. *Parkinsonism & Related Disorders, 30*, 46–51. https://doi.org/10.1016/j.parkreldis.2016.06.018.

Hermann, W. (2014). Morphological and functional imaging in neurological and non-neurological Wilson's patients. *Annals of the New York Academy of Sciences, 1315*, 24–29. https://doi.org/10.1111/nyas.12343.

Hu, X., Chen, S., Huang, C. B., Qian, Y., & Yu, Y. (2017). Frequency-dependent changes in the amplitude of low-frequency fluctuations in patients with Wilson's disease: A resting-state fMRI study. *Metabolic Brain Disease, 32*(3), 685–692. https://doi.org/10.1007/s11011-016-9946-3.

Hua, K., Zhang, J., Wakana, S., Jiang, H., Li, X., Reich, D. S., Calabresi, P. A., Pekar, J. J., van Zijl, P. C., & Mori, S. (2008). Tract probability maps in stereotaxic spaces: Analyses of white matter anatomy and tract-specific quantification. *NeuroImage, 39*(1), 336–347. https://doi.org/10.1016/j.neuroimage.2007.07.053.

Jadav, R., Saini, J., Sinha, S., Bagepally, B., Rao, S., & Taly, A. B. (2013). Diffusion tensor imaging (DTI) and its clinical correlates in drug naïve Wilson's disease. *Metabolic Brain Disease, 28*(3), 455–462. https://doi.org/10.1007/s11011-013-9407-1.

Jing, R., Han, Y., Cheng, H., Han, Y., Wang, K., Weintraub, D., & Fan, Y. (2019). Altered large- scale functional brain networks in neurological Wilson's disease. *Brain imaging and behavior*, https://doi.org/10.1007/s11682-019-00066-y. advance online publication. https://doi.org/10.1007/s11682-019-00066-y.

Kalita, J., Kumar, V., Misra, U. K., & Bora, H. K. (2018). Memory and learning dysfunction following copper toxicity: Biochemical and Immunohistochemical basis. *Molecular Neurobiology, 55*(5), 3800–3811. https://doi.org/10.1007/s12035-017-0619-y.

Karantzoulis, S., Novitski, J., Gold, M., & Randolph, C. (2013). The repeatable battery for the assessment of neuropsychological status (RBANS): Utility in detection and characterization of mild cognitive impairment due to Alzheimer's disease. *Archives of clinical neuropsychology: the official journal of the National Academy of Neuropsychologists, 28*(8), 837–844. https://doi.org/10.1093/arclin/act057.

Kozić, D., Svetel, M., Petrović, B., Dragasević, N., Semnic, R., & Kostić, V. S. (2003). MR imaging of the brain in patients with hepatic form of Wilson's disease. *European Journal of Neurology, 10*(5), 587–592. https://doi.org/10.1046/j.1468-1331.2003.00661.x.

Lin, W., Chen, X., Gao, Y. Q., Yang, Z. T., Yang, W., & Chen, H. J. (2019). Hippocampal atrophy and functional connectivity disruption in cirrhotic patients with minimal hepatic encephalopathy. *Metabolic Brain Disease, 34*(6), 1519–1529. https://doi.org/10.1007/s11011-019-00457-6.

Litwin, T., Dzieżyc, K., Karliński, M., Chabik, G., Czepiel, W., & Członkowska, A. (2015). Early neurological worsening in patients with Wilson's disease. *Journal of the Neurological Sciences, 355*(1–2), 162–167. https://doi.org/10.1016/j.jns.2015.06.010.

Litwin, T., Gromadzka, G., Członkowska, A., Gołębiowski, M., & Poniatowska, R. (2013). The effect of gender on brain MRI pathology in Wilson's disease. *Metabolic Brain Disease, 28*(1), 69–75. https://doi.org/10.1007/s11011-013-9378-2.

Magalhaes, A. C., Caramelli, P., Menezes, J. R., Lo, L. S., Bacheschi, L. A., Barbosa, E. R., Rosemberg, L. A., & Magalhaes, A. (1994). Wilson's disease: MRI with clinical correlation. *Neuroradiology, 36*(2), 97–100. https://doi.org/10.1007/BF00588068.

Mosher, V., Swain, M. G., Pang, J., Kaplan, G. G., Sharkey, K. A., MacQueen, G. M., & Goodyear, B. G. (2017). Primary biliary cholangitis alters functional connections of the Brain's deep gray matter. *Clinical and Translational Gastroenterology, 8*(7), e107. https://doi.org/10.1038/ctg.2017.34.

Mosher, V., Swain, M., Pang, J., Kaplan, G., Sharkey, K., MacQueen, G., & Goodyear, B. G. (2019). Primary biliary cholangitis patients exhibit MRI changes in structure and function of interoceptive brain regions. *PLoS One, 14*(2), e0211906. https://doi.org/10.1371/journal.pone.0211906.

Pal, A., & Prasad, R. (2014). Recent discoveries on the functions of astrocytes in the copper homeostasis of the brain: A brief update. *Neurotoxicity Research, 26*(1), 78–84. https://doi.org/10.1007/s12640-013-9453-9.

Papademetris, X., Jackowski, A. P., Schultz, R. T., Staib, L. H., & Duncan, J. S. (2001). Integrated intensity and point-feature nonrigid registration. *Medical image computing and computer-assisted intervention : MICCAI ... International Conference on Medical Image Computing and Computer-Assisted Intervention*, *3216*(2004), 763–770. https://doi.org/10.1901/jaba.2001.3216-763.

Papademetris, X., Jackowski, M. P., Rajeevan, N., DiStasio, M., Okuda, H., Constable, R. T., & Staib, L. H. (2006). BioImage suite: An integrated medical image analysis suite: An update. *The insight journal, 2006*, 209.

Prashanth, L. K., Taly, A. B., Sinha, S., Ravishankar, S., Arunodaya, G. R., Vasudev, M. K., & Swamy, H. S. (2005). Prognostic factors in patients presenting with severe neurological forms of Wilson's disease. *QJM : Monthly Journal of the Association of Physicians, 98*(8), 557–563. https://doi.org/10.1093/qjmed/hci095.

Randolph, C., Tierney, M. C., Mohr, E., & Chase, T. N. (1998). The repeatable battery for the assessment of neuropsychological status (RBANS): Preliminary clinical validity. *Journal of Clinical and Experimental Neuropsychology, 20*(3), 310–319. https://doi.org/10.1076/jcen.20.3.310.823.

Schilsky, M. L. (2017). Wilson disease: Diagnosis, treatment, and follow-up. *Clinics in Liver Disease, 21*(4), 755–767. https://doi.org/10.1016/j.cld.2017.06.011.

Shen, X., Tokoglu, F., Papademetris, X., & Constable, R. T. (2013). Groupwise whole-brain parcellation from resting-state fMRI data for network node identification. *NeuroImage, 82*, 403–415. https://doi.org/10.1016/j.neuroimage.2013.05.081.

Sinha, S., Taly, A. B., Prashanth, L. K., Ravishankar, S., Arunodaya, G. R., & Vasudev, M. K. (2007). Sequential MRI changes in Wilson's disease with de-coppering therapy: A study of 50 patients. *The British Journal of Radiology, 80*(957), 744–749. https://doi.org/10.1259/bjr/48911350.

Smolinski, L., Litwin, T., Redzia-Ogrodnik, B., Dziezyc, K., Kurkowska-Jastrzebska, I., & Czlonkowska, A. (2019). Brain volume is related to neurological impairment and to copper overload in Wilson's disease. *Neurological sciences : official journal of the Italian Neurological Society and of the Italian Society of Clinical Neurophysiology, 40*(10), 2089–2095. https://doi.org/10.1007/s10072-019-03942-z.

Stezin, A., George, L., Jhunjhunwala, K., Lenka, A., Saini, J., Netravathi, M., Yadav, R., & Pal, P. K. (2016). Exploring cortical atrophy and its clinical and biochemical correlates in Wilson's disease using voxel based morphometry. *Parkinsonism & Related Disorders, 30*, 52–57. https://doi.org/10.1016/j.parkreldis.2016.06.017.

Strauss, E., Sherman, E. M. S., & Spreen, O. (2006). *A compendium of neuropsychological tests: Administration, norms, and commentary* (3rd ed.). New York: Oxford University Press.

Südmeyer, M., Saleh, A., Wojtecki, L., Cohnen, M., Gross, J., Ploner, M., Hefter, H., Timmermann, L., & Schnitzler, A. (2006). Wilson's disease tremor is associated with magnetic resonance imaging lesions in basal ganglia structures. *Movement disorders : official journal of the Movement Disorder Society, 21*(12), 2134–2139. https://doi.org/10.1002/mds.21136.

Tarnacka, B., Szeszkowski, W., Buettner, J., Gołebiowski, M., Gromadzka, G., & Członkowska, A. (2009). Heterozygous carriers for Wilson's disease–magnetic spectroscopy changes in the brain. *Metabolic Brain Disease, 24*(3), 463–468. https://doi.org/10.1007/s11011-009-9145-6.

Terwel, D., Löschmann, Y. N., Schmidt, H. H., Schöler, H. R., Cantz, T., & Heneka, M. T. (2011). Neuroinflammatory and behavioural changes in the Atp7B mutant mouse model of Wilson's disease. *Journal of Neurochemistry, 118*(1), 105–112. https://doi.org/10.1111/j.1471-4159.2011.07278.x.

Tombaugh, T. N. (2004). Trail making test a and B: Normative data stratified by age and education. *Archives of clinical neuropsychology : the official journal of the National Academy of Neuropsychologists, 19*(2), 203–214. https://doi.org/10.1016/S0887-6177(03)00039-8.

Tombaugh, T. N., Kozak, J., & Rees, L. (1999). Normative data stratified by age and education for two measures of verbal fluency: FAS and animal naming. *Archives of clinical neuropsychology : the official journal of the National Academy of Neuropsychologists, 14*(2), 167–177.

Torres, D. S., Abrantes, J., & Brandão-Mello, C. E. (2013). Cognitive assessment of patients with minimal hepatic encephalopathy in Brazil. *Metabolic Brain Disease, 28*(3), 473–483. https://doi.org/10.1007/s11011-013-9405-3.

Wakana, S., Caprihan, A., Panzenboeck, M. M., Fallon, J. H., Perry, M., Gollub, R. L., Hua, K., Zhang, J., Jiang, H., Dubey, P., Blitz, A., van Zijl, P., & Mori, S. (2007). Reproducibility of quantitative tractography methods applied to cerebral white matter. *NeuroImage, 36*(3), 630–644. https://doi.org/10.1016/j.neuroimage.2007.02.049. Walshe, J. M., & Yealland, M. (1993). Chelation treatment of neurological Wilson's disease. *The Quarterly Journal of Medicine, 86*(3), 197–204. Whitfield-Gabrieli, S., & Nieto-Castanon, A. (2012). Conn: A functional connectivity toolbox for correlated and anticorrelated brain networks. *Brain Connectivity, 2*(3), 125–141. https://doi.org/10.1089/brain.2012.0073. Yang, J., Li, X., Yang, R., Yu, X., Yu, C., Qian, Y., & Yu, Y. (2015). Susceptibility-weighted imaging manifestations in the brain of Wilson's disease patients. *PLoS One, 10*(4), e0125100. https://doi.org/10.1371/journal.pone.0125100. Zhou, X. X., Li, X. H., Qin, H., Li, G. D., Huang, H. W., Liang, Y. Y., Liang, X. L., & Pu, X. Y. (2016). Diffusion tensor imaging of the extracorticospinal network in the brains of patients with Wilson disease. *Journal of the Neurological Sciences, 362*, 292–298. https://doi.org/10.1016/j.jns.2016.02.006. Zhong, W., Huang, Z., & Tang, X. (2019). A study of brain MRI characteristics and clinical features in 76 cases of Wilson's disease. *Journal of clinical neuroscience: official journal of the Neurosurgical Society of Australasia, 59*, 167–174. https://doi.org/10.1016/j.jocn.2018.10.096. Zou, L., Song, Y., Zhou, X., Chu, J., & Tang, X. (2019). Regional morphometric abnormalities and clinical relevance in Wilson's disease. *Movement disorders: official journal of the Movement Disorder Society, 34*(4), 545–554. https://doi.org/10.1002/mds.27641.